J|A|C|S
ARTICLES

Published on Web 03/19/2009

# Real-Time NMR Investigations of Structural Changes in Silicon Electrodes for Lithium-Ion Batteries

Baris Key,[†] Rangeet Bhattacharyya,[†] Mathieu Morcrette,[‡] Vincent Seznéc,[‡] Jean-Marie Tarascon,[‡] and Clare P. Grey*[,†]

*Department of Chemistry, SUNY at Stony Brook, Stony Brook, New York 11794-3400, and LRCS, CNRS-UMR6007 Université de Picardie Jules Verne, 33 Rue Saint Leu 80039, Amiens, France*

Received November 3, 2008; E-mail: cgrey@notes.cc.sunysb.edu

***Abstract:*** Lithium-ion batteries (LIBs) containing silicon negative electrodes have been the subject of much recent investigation because of the extremely large gravimetric and volumetric capacity of silicon. The crystalline-to-amorphous phase transition that occurs on electrochemical Li insertion into crystalline Si, during the first discharge, hinders attempts to link structure in these systems with electrochemical performance. We apply a combination of static, in situ and magic angle sample spinning, ex situ $^{7}$Li nuclear magnetic resonance (NMR) studies to investigate the changes in local structure that occur in an actual working LIB. The first discharge occurs via the formation of isolated Si atoms and smaller Si−Si clusters embedded in a Li matrix; the latter are broken apart at the end of the discharge, forming isolated Si atoms. A spontaneous reaction of the lithium silicide with the electrolyte is directly observed in the in situ NMR experiments; this mechanism results in self-discharge and potential capacity loss. The rate of this self-discharge process is much slower when CMC (carboxymethylcellulose) is used as the binder.

## 1. Introduction

Rechargeable lithium-ion batteries (LIBs) are currently the most preferred energy storage devices in portable electronic devices, having the highest gravimetric and volumetric energy densities. Their potential use in hybrid and plug-in hybrid electric vehicles and all-electric vehicles (HEVs, PHEVs and EVs) make advances in this field the more significant, due to both economic and environmental implications. The universally used negative electrode material in a LIB is carbon because of its good capacity (372 mA h $g^{-1}$ for graphite) and rate capability. However, new, low cost, safe electrode materials with higher capacities are still urgently required for both portable and transportation applications. To this end, tin-based anodes with large, theoretical volumetric and gravimetric capacities have recently been commercialized in Sony's NEXELION cells. Silicon anodes are particularly attractive alternatives to carbon with extremely high gravimetric energy densities (3572 mA h $g^{-1}$). Compared to graphite, silicon has a massive volumetric capacity of 8322 mA h $cm^{-3}$ (calculated based on the original volume of silicon) which is approximately 10 times that of graphite. However, the unusually high capacity is associated with large electrode volume changes of up to 300%, resulting in particle fracture and capacity retention issues, along with design challenges, since the expansion has to be managed in the cell. Previous work has proposed two main solutions to overcome these problems: (i) using composite electrodes of silicon and carbon, coated with a binder such as CMC (carboxymethylcellulose), to maintain particle−particle contact after many charge/discharge cycles; (ii) limiting the voltages over which the material is cycled, thereby limiting the extent of volumetric expansion by sacrificing some capacity.[1−4] The use of nanoparticles of Si also appears to improve capacity retention.[4−6] Such attempts to improve the Si electrode performance and long-term capacity retention may result in the commercialization of a next generation of Li-ion batteries with silicon negative electrodes in the near future.

The binary phase diagram of Li−Si system consists of four reported crystalline lithium silicides, from $Li_{12}Si_7$, to the increasingly lithium-rich phases $Li_7Si_3$, $Li_{13}Si_4$ and $Li_{21}Si_5$ (Figure 1).[7−13] However, at room temperature, silicon does not form any of these phases on electrochemical lithiation, but

[†] SUNY at Stony Brook.
[‡] LRCS, CNRS-UMR6007 Université de Picardie Jules Verne.

(1) Hochgatterer, N. S.; Schweiger, M. R.; Koller, S.; Raimann, P. R.; Woehrle, T.; Wurm, C.; Winter, M. *Electrochem. Solid State Lett.* **2008**, *11*, A76−A80.
(2) Li, J.; Christensen, L.; Obrovac, M. N.; Hewitt, K. C.; Dahn, J. R. *J. Electrochem. Soc.* **2008**, *155*, A234−A238.
(3) Obrovac, M. N.; Krause, L. J. *J. Electrochem. Soc.* **2007**, *154*, A103−A108.
(4) Holzapfel, M.; Buqaa, H.; Hardwick, L. J.; Hahna, M.; Würsig, A.; Scheifele, W.; Novák, P.; Kötz, R.; Veit, C.; Petrat, F.-M. *Electrochim. Acta* **2006**, *52*, 973–978.
(5) Li, H.; Huang, X.; Chen, L.; Wu, Z.; Liang, Y. *Electrochem. Solid State Lett.* **1999**, *2*, 547–549.
(6) Chan, C. K.; Peng, H.; Liu, G.; McIlwrath, K.; Zhang, X. F.; Huggins, R. A.; Cui, Y. *Nat. Nanotechnol.* **2008**, *3*, 31–35.
(7) Nesper, R. *Prog. Solid State Chem.* **1990**, *20*, 1–45.
(8) Schnering, H. G. v.; Nesper, R.; Curda, J.; Tebbe, K.-F. *Angew. Chem.* **1980**, *92*, 1070–1071.
(9) Nesper, R.; Schnering, H. G. v.; Curda, J. *Chem. Ber.* **1986**, *119*, 3576–3590.
(10) Klemm, W.; Struck, M. *Z. Anorg. Chem.* **1955**, *278*, 117–121.
(11) Schnering, H. G. V.; Nesper, R.; Tebbe, K. F.; Curda, J. *Z. Metallkd.* **1980**, *71*, 357–363.
(12) Frank, U.; Muller, W.; Schafer, H. *Z. Naturforsch.* **1975**, *30b*, 10–13.
(13) Nesper, R.; Schnering, H. G. v. *J. Solid State Chem.* **1987**, *70*, 48–57.

10.1021/ja8086278 CCC: $40.75 

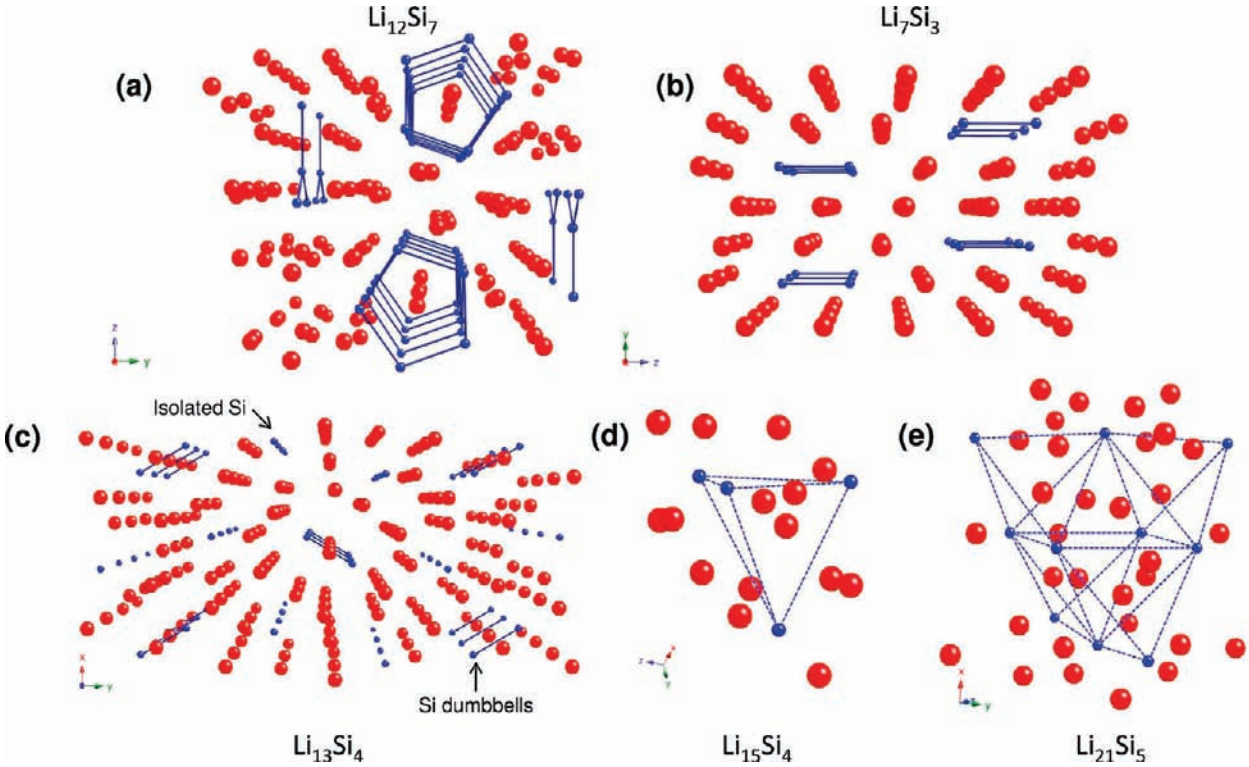


***Figure 1.*** Structural representations of (a) $Li_{12}Si_7$, 13 Li and 9 Si crystallographic sites, (Si−Si distances in rings and stars, 2.35−2.40 Å),[7−9] (b) $Li_7Si_3$, 3 Li and 1 Si sites, (Si−Si dumbbell distances, 2.332 Å),[7,10,11] (c) $Li_{13}Si_4$, 8 Li and 2 Si sites, (Si−Si dumbbells, 2.383 Å and isolated silicon ions),[7,12] (d) $Li_{15}Si_4$, 2 Li and 1 Si sites (isolated silicon ions, Si−Si distances >4.5 Å),[15] and (e) $Li_{21}Si_5$, 16 Li and 4 Si sites, (Si−Si distances >4.6 Å).[7,13] (Li and Si atoms are shown in red and blue, respectively; blue lines: Si−Si bonds; blue dashed lines: closest Si−Si contacts > than 3.0 Å).

instead undergoes a crystalline to amorphous phase transition, forming a lithiated amorphous silicide.[14] This phase then recrystallizes at deep discharge to form a metastable phase, $Li_{15}Si_4$, which is isostructural to the thermodynamic phase, $Li_{15}Ge_4$.[15] This final composition provides the theoretical capacity of 3.75 Li per Si (3572 mA h $g^{-1}$). Interestingly, lithiated nanoparticles of crystalline and amorphous thin films less than 2 $\mu$m thickness of silicon do not recrystallize at deep discharge.[16,17] Unfortunately, due to the amorphous nature of the lithiated silicides, it is not possible to monitor all the structural changes that occur during lithium insertion/removal with conventional methods such as diffraction. The short-range order of the amorphous materials remains unknown, preventing attempts to optimize performance based on electrochemical-structure correlations.

Although nuclear magnetic resonance (NMR) spectroscopy has been used to obtain detailed local structural information from battery materials,[18] it has not been widely used to study batteries under realistic operating conditions. The first in situ NMR experiments of batteries were performed by Gerald et al. in[19] where an NMR toroid cavity was used for both in situ NMR and for imaging. However, a poor signal-to-noise ratio was obtained, and furthermore, the toroid design was difficult to combine with a standard LIB. More recent in situ experiments were performed by Letellier et al. to examine the insertion reaction of Li in disordered carbon and graphitic anodes by $^7$Li NMR spectroscopy making use of a so-called plastic lithium-ion battery.[20,21] This battery design is advantageous because the battery is flexible and does not require external pressure to maintain contact between the cathode, electrolyte and anode. Both sets of experiments (the toroid and plastic-bag designs) were performed in static mode, i.e., without magic angle spinning (MAS).

In this report we utilize a flexible plastic LIB design and a combination of static, in situ and MAS, ex situ $^7$Li and $^{29}$Si NMR spectroscopy as local structural probes in order to monitor/identify the changes in the short-range order that occur during the first discharge of crystalline silicon in an actual working LIB. We demonstrate that in situ $^7$Li NMR experiments can be used to capture changes that cannot be readily seen by ex situ methods. In order to correlate Li NMR shifts with specific local environments, we first acquired the $^7$Li MAS NMR spectra of the crystalline phases $Li_{12}Si_7$, $Li_7Si_3$, $Li_{13}Si_4$, $Li_{15}Si_4$ and $Li_{21}Si_5$. The Li NMR shifts associated with specific Li local environments and types of silicon clusters were then used to help determine the structural changes that occur on discharge of the Si−Li battery.

(14) Limthongkul, P.; Jang, Y.-I.; Dudney, N. J.; Chiang, Y.-M. *J. Power Sources* **2003**, *119−121*, 604–609.
(15) Obrovac, M. N.; Christensen, L. *Electrochem. Solid State Lett.* **2004**, *7*, A93−A96.
(16) Li, H.; Huang, X.; Chen, L.; Zhou, G.; Zhang, Z.; Yu, D.; Mo, Y. J.; Pei, N. *Solid State Ionic* **2000**, *135*, 181–191.
(17) Hatchard, T. D.; Dahn, J. R. *J. Electrochem. Soc.* **2004**, *151*, A838−A842.
(18) Grey, C. P.; Dupre, N. *Chem. Rev.* **2004**, *104*, 4493–4512.
(19) Gerald, R. E.; Klingler, R. J.; Sandi, G.; Johnson, C. S.; Scanlon, L. G.; Rathke, J. W. *J. Power Sources* **2000**, *89*, 237–243.
(20) Chevallier, F.; Letellier, M.; Morcrette, M.; Tarascon, J.-M.; Frackowiak, E.; Rouzaud, J.-N.; Beguin, F. *Electrochem. Solid State Lett.* **2003**, *6*, A225−A228.
(21) Letellier, M.; Chevallier, F.; Morcrette, M. *Carbon* **2007**, *45*, 1025–1034.

## 2. Experimental Section

**2.1. Synthesis of Model Compounds.** The lithium silicides were synthesized by mixing stoichiometric amounts of lithium metal and silicon 325 (Aldrich) mesh powder in an argon glovebox. The mixtures were sealed in an inert atmosphere and ball-milled out of the glovebox for 8 h. The containers were transferred back into the glovebox, sealed in inox (stainless-steel) containers, and then annealed for 12 h at 450 °C for $Li_{12}Si_7$ and $Li_{21}Si_5$ and at 500 °C for $Li_7Si_3$ and $Li_{13}Si_4$. $Li_{15}Si_4$, however, was not annealed since it is a metastable phase; annealing led to the decomposition of this material, forming a mixture of unidentified (likely, metastable) phases.

**2.2. Diffraction.** All the diffraction patterns of the model compounds were acquired with a Bruker D8 advance diffractometer (Cu Kα radiation, $\theta$-$2\theta$ geometry, Vantec counter). An airtight swagelok cell with a beryllium window was used, as described in ref 22.

**2.3. Electrochemistry.** For all the ex situ NMR samples prepared in this study, 2032 type coin cells were used following a standard assembly procedure: The positive electrode was either pure crystalline silicon powder (325 mesh, Aldrich) or the $Li_{15}Si_4$ model compound, mixed with super P carbon in 1:1 weight ratio, and the negative electrode was lithium metal (0.38 mm thickness). 1 M $LiPF_6$ dissolved in a 1:1 volumetric mixture of anhydrous ethylene carbonate (EC) and anhydrous dimethyl carbonate (DMC) was used as the electrolyte (Merck, Selectipur). A porous glass fiber soaked with the electrolyte was used as the separator. The cells were assembled in an argon glovebox and cycled galvanostatically between potential limits of 3.0−0.0 V at a C/150 discharge rate with an Arbin Instruments galvanostat/potentiostat at room temperature. After electrochemical cycling, the cells were dissembled in the glovebox where the active materials were extracted, dried and packed into 1.8 mm diameter zirconia rotors for MAS NMR analysis.

For the in situ NMR studies, a flexible battery design, modified from Bellcore's plastic lithium-ion battery technology[20] was used. The positive electrodes were prepared by mixing 37:37:10:16 weight ratio of crystalline silicon (325 mesh, Aldrich), super P carbon, poly vinylidene fluoride (PVDF) and dibutyl phthalate (DBP). The mixture was mixed with acetone to prepare a slurry, which was then spread evenly (1 mm) over a flat surface. The dried film of approximate 150 $\mu$m thickness (and area 12 mm × 10 mm) was then laminated on carbon-coated copper wire mesh (by heating at 135 °C with 20 psi vertical pressure), leaving unlaminated copper mesh at one end to serve as the battery leads. A small strip was cut from the larger electrode with an area of approximately 3 mm × 10 mm. The negative electrode was prepared by pressing lithium metal (0.38 mm thickness) onto copper wire mesh, in a glovebox, again leaving bare copper mesh for the battery leads (Figure 2a). The electrolyte used in this study was 1 M $LiPF_6$ dissolved in a 1:1 volumetric mixture of anhydrous EC and anhydrous DMC. A porous glass fiber soaked with the electrolyte was used as a separator.

The cell components were assembled in a polyethylene bag (Figure 2a) which was hermetically sealed inside an argon glovebox. The final dimensions of the cell electrodes were 10 × 4 mm (area) × approximately 2 mm (height). The flexible cell was then placed tightly inside the 5 mm coil of a conventional CMX static probe (Figure 2b). An Arbin Instruments galvanostat/potentiostat was used for cycling the battery in situ. Low-pass filters (50 MHz) were used to filter the high-frequency noise coming from the cycler to improve the signal-to-noise ratio of the NMR spectrum.[20] The in situ cell was cycled galvanostatically between 3.0 and 0.0 V during the spectral acquisition.

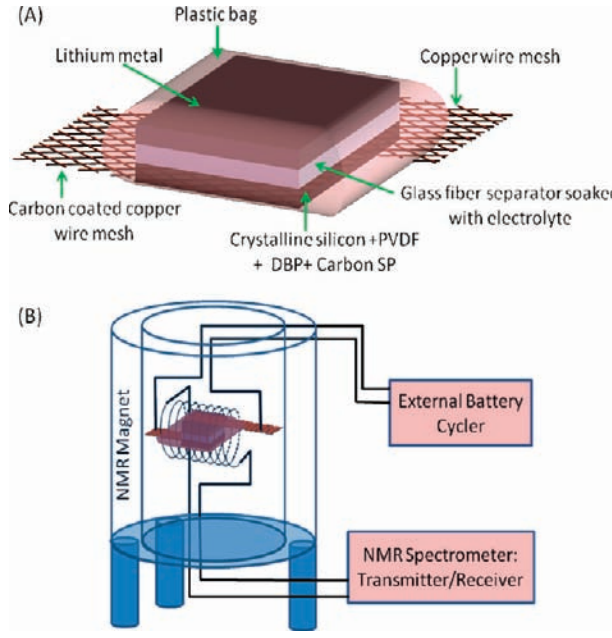


***Figure 2.*** (a) Schematics of the flexible plastic battery used for the in situ static NMR experiment and (b) the in situ static NMR setup.

**2.4. NMR: Model Compounds and ex Situ Battery Samples.** $^7$Li MAS NMR spectra were acquired at 77.63 MHz using a CMX-200 MHz spectrometer, with a 1.8 mm MAS probe at a 38 kHz spinning speed. All the $^7$Li spectra were referenced to a 1 M LiCl solution at 0 ppm. Rotor-synchronized spin−echoes (90° − $\tau$ − 180° − $\tau$ − acq) were used to acquire the spectra, where the values of $\tau$ were chosen, such that they were equal to the rotor period (i.e., $\tau$ = 1/spinning frequency). A recycle delay of 0.2 s was used to collect a total of 32000 scans for each sample. Presaturation experiments were employed to determine whether the various signals originate from the same or multiple phases.[23] These experiments involve applying a long, low-power, frequency-selective irradiation on a chosen resonance, to destroy the magnetization of the spins giving rise to this resonance, and to perturb the resonances arising from the spins that are connected to the original spins, either via dipolar coupling or chemical-exchange mechanisms. This weak pulse is then followed by a mixing delay ($\tau_m$, typically 1 ms, much shorter than the shortest spin−lattice relaxation time, $T_1$), to further enhance any possible exchange between local environments in the same phase. A hard pulse is then used to excite the whole sample, and the signal is then acquired. If all the isotropic resonances remain undistorted, except the original irradiated resonance, this provides strong evidence that the selected resonance originates from spins in a separate phase.

**2.5. In situ NMR.** The static $^7$Li NMR spectra were acquired at 77.63 MHz using an Infinity-200 MHz spectrometer (Figure 2b). A single pulse sequence was used with flip angles of 90° to collect a total of 5000 scans for each spectrum. A recycle delay of 0.2 s was used for the discharge/charge experiment and for the relaxation experiment involving a second battery stopped at the end of the first discharge.

**2.6. $^{29}$Si MAS NMR Spectra.** These were acquired at 71.55 MHz using a CMX-360 MHz spectrometer with a 4.0 mm MAS probe at a 14 kHz spinning speed. The $^{29}$Si NMR spectra were referenced to tetramethylsilane (TMS) (at 0 ppm) as an external reference. Spin−echoes (90° − $\tau$ − 180° − $\tau$ − acq) were used to acquire the spectra. To enhance the signal-to-noise of some samples, the CPMG (Carr−Purcell−Meibohm and Gill) experiment,[24] with a pulse sequence comprising of a series of

(22) Morcrette, M.; Chabre, Y.; Vaughan, G.; Amatucci, S.; Leriche, J.-B.; Patoux, S.; Masquelier, C.; Tarascon, J.-M. *Electrochem. Acta* **2002**, *47*, 3137–3149.

(23) Kuhns, P. L.; Conradi, M. S. *J. Chem. Phys.* **1982**, *77*, 1771–1778.
(24) Carr, H. Y.; Purcell, E. M. *Phys. Rev.* **1954**, *94*, 630–638.

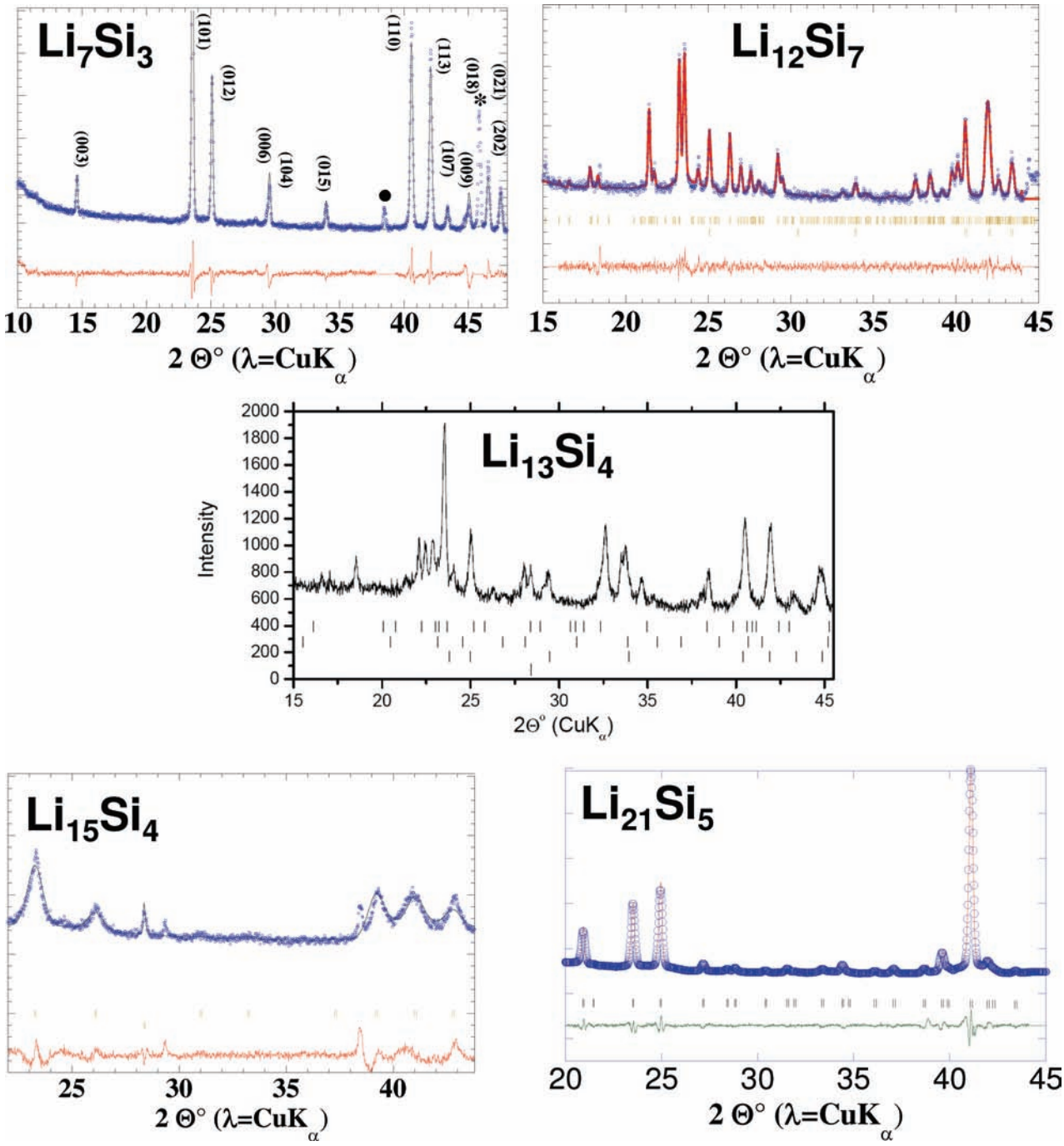


***Figure 3.*** X-ray diffraction patterns of lithium silicide intermetallic compounds. Fittings of four of the patterns, performed using the *Fullprof* software in profile-matching mode, are shown; the difference between the experimental data and the fit is shown underneath each pattern. The tick marks represent the reflections for respective structure models and impurity phases. The second set of tickmarks in $Li_{15}Si_4$ and $Li_{12}Si_7$ represent Si and $Li_2Si$. For $Li_{13}Si_4$, tickmarks are shown for the $Li_{13}Si_4$ (top; major phase), $Li_{21}Si_5$ (top middle), $Li_7Si_3$ (bottom middle) and Si (bottom); the remaining unindexed peaks correspond to unknown phases. * = Be; filled circle = Al.

spin−echoes ($90° - \tau - n \times [180° -$ acquisition $(2\tau)]$), was used. The number of 180° pulses ($n$) was chosen to acquire the maximum number of echoes permitted by the spin−spin relaxation time ($T_2$). The sequence was rotor synchronized with the value of $\tau$ being chosen, such that it was equal to the rotor period (i.e., $\tau$ = 1/frequency of spinning). A recycle delay of 1 s was used. The one pulse spectra took approximately 2 days to acquire, due to the low natural abundance of $^{29}Si$ (4.67%), the CPMG spectra taking only 36 h. To maximize the signal-to-noise level, the spectral width of each spectrum was minimized so as to cover only the range containing the resonances.

## 3. Results and Discussion

**3.1. Model Compounds. 3.1.1. Diffraction.** The diffraction patterns of all the model compounds and profile fittings of selected compounds are shown in Figure 3. The majority of the synthesized compounds were largely impurity free except the minor unreacted Si phase in $Li_{15}Si_4$, and very minor impurities (including $Li_2Si$) in $Li_{12}Si_7$. $Li_{13}Si_4$, however, does contain a number of impurities, including $Li_{21}Si_5$, $Li_{12}Si_7$ and a weaker unidentified (unreported) impurity phase(s).

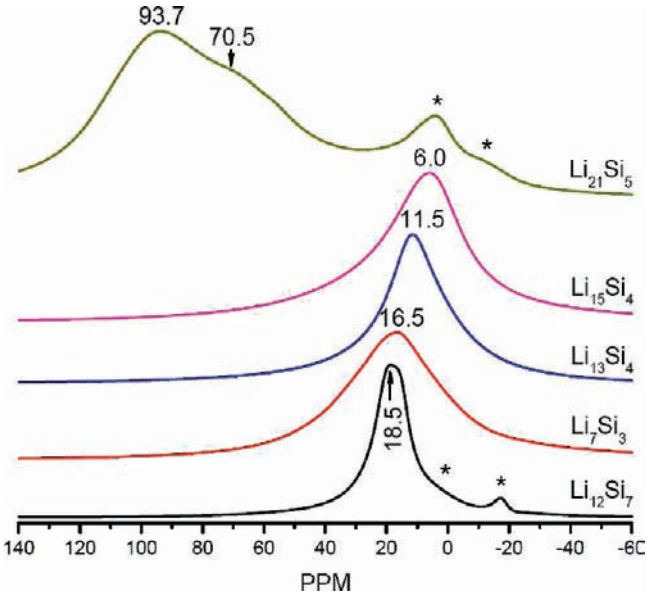


***Figure 4.*** $^{7}$Li MAS NMR spectra of $Li_{12}Si_7$, $Li_7Si_3$, $Li_{13}Si_4$, $Li_{15}Si_4$ and $Li_{21}Si_5$ at a spinning speed of 38 kHz. Impurity phases are marked with asterisks (*).

**3.1.2. NMR.** The $^{7}$Li MAS NMR spectra of the model compounds $Li_{12}Si_7$, to the increasingly lithium-rich phases $Li_7Si_3$, $Li_{13}Si_4$, $Li_{15}Si_4$ and $Li_{21}Si_5$ are shown in Figure 4. These materials lie on the border between so-called Zintl phases and intermetallic compounds. Their structures cannot be easily rationalized by using simple Zintl−Klemm electron-counting concepts, as discussed in a recent review (see Supporting Information), but contain additional orbital(s) delocalized over multiple lithium ions.[6] The $^{7}$Li MAS NMR spectrum (Figure 4) of the Li-rich end member, $Li_{21}Si_5$, is distinct: Among the known thermodynamic phases, $Li_{21}Si_5$ is the only phase that is reported to be metallic, the others being semiconductors.[7−13] The large shifts of the broad, overlapping resonances (at approximately 100−60 ppm) seen in this material are ascribed to the Knight shift, which is a measure of the density of states at the Fermi level at the Li nucleus. The weaker resonances centered at approximately 4.8 ppm are due to Li in more shielded and/or less metallic/semiconducting environments and are ascribed to impurity phases. $^{7}$Li NMR presaturation experiments were performed to confirm this hypothesis, by irradiating either the 70−94 ppm peaks or the 4−0 ppm groups of peaks with a weak radio frequency field. This method saturates all the signals from environments that are in close spatial proximity (and thus magnetically coupled, e.g., via $^{7}$Li−$^{7}$Li dipolar couplings). In either case, irradiation of one set of peaks (even for as much as 20 ms) did not affect the other set of peaks, suggesting that they are not part of the same phase. Although no impurity Li-containing phases were seen by XRD for this Material, the presence of additional NMR resonances in its $^{7}$Li spectrum is ascribed to amorphous components not seen by XRD, and the formation of new phases on partial exposure of the materials to trace amounts of oxygen that may have leaked into the rotor during the NMR experiment. We note however, that we were careful to examine the NMR spectra of all of the materials studied in this work immediately and then following more extended data acquisition, to ensure that the spectra presented in this paper were not affected by oxygen contamination. Furthermore, we ran the spectra of the model compounds and many of the battery samples discussed below on at least two occasions to ensure reproducibility. Only the spectra of $Li_{21}Si_5$ showed some evidence for possible contamination/decomposition of the sample.

All of the other lithium silicides exhibit resonances at much lower frequencies than those of $Li_{21}Si_5$, indicating quite different electronic properties (Figure 4). A clear trend is observed for these resonances, their shifts moving to lower frequencies as the Li/Si ratio increases and the shielding (electron density) on the Li ion increases. The most lithium-deficient phase $Li_{12}Si_7$ contains planar $Si_5$ rings and trigonal-planar "star type" $Si_4$ clusters,[7−9] the $Li^+$ surrounding these clusters giving rise to resonances centered at approximately 18.5 ppm. The peaks at 2 ppm and −17.6 ppm are ascribed to minor impurities, presumably amorphous phases. $Li_7Si_3$ contains $Si_2$ dumbbells, the average partial charges on the Li ions decreasing,[10,11] causing a shift of the center of mass of this spectrum to 16.5 ppm. $Li_{13}Si_4$ contains both Si−Si dumbbells and isolated silicon $Si^{4-}$ ions, and the shift of the NMR signal to lower frequencies (11.5 ppm) is consistent with increase in the Li/Si ratio. Presumably a combination of slow lithium-ion motion, residual $^{7}$Li dipolar coupling, and possibly disorder prevents resolution of the resonances from the three crystallographic sites. The NMR signal from $Li_{15}Si_4$ is not affected by the large Knight shifts that were observed in $Li_{21}Si_5$ spectrum. Instead, the homogeneous distribution of Si ions in the Li matrix gives rise to the most shielded Li environment(s), resulting in a broad resonance at 6.0 ppm. Thus, in conclusion, the most deshielded Li environments with peaks around 16−18 ppm are found in structures containing Si−Si bonds (rings/clusters/dumbbells), while the more shielded environments found for isolated silicon ions resonate at around 6.0 ppm, intermediate shifts being observed for compounds containing both types of structural motifs. These correlations are now used to help elucidate the structural changes that occur on electrochemical lithiation of Si.

**3.2. NMR Spectroscopy of Li−Si batteries. 3.2.1. Ex Situ NMR.** The electrochemical profile for the first discharge of a crystalline silicon (vs $Li^+$/Li) battery, fully discharged over 150 h (C/150 rate) shows two distinct regions (at approximately 800 mV and below 110 mV) (Figure 5a). Note that, since the theoretical capacity of Si is so large, the current used to achieve a C/150 rate, 24 mA $g^{-1}$, corresponds to the same current used when cycling a Li/graphite cell at approximately C/15. The significant capacity (500 mA h $g^{-1}$) that is observed above 110 mV is largely due to the irreversible reaction of amorphous carbon in the electrode mixture (present in a 1:1 weight ratio with silicon. This is consistent with the in situ X-ray diffraction (XRD) data (see Supporting Information), where no intensity changes involving the Si are observed in this voltage region. (N.b., given that this represents a fundamental study of the Si reaction processes, we deliberately chose to use a high carbon content in the electrode mixtures so as to ensure good/consistent reactivity of the Si.) The Si reflections drop steadily in intensity during the second plateau-like region, but no new phases are observed. An analysis of the rate of change of intensity gives a composition of the amorphous phase of approximately $Li_{3.4\pm0.2}Si$. Only at the very end of discharge is the crystalline $Li_{15}Si_4$ phase seen by both in- and ex situ XRD[14,23,24] (and see Supporting Information).

To investigate the different voltage regions in detail with $^{7}$Li MAS NMR spectroscopy, nine coin cells composed of crystalline silicon as the positive electrode and lithium metal as the negative

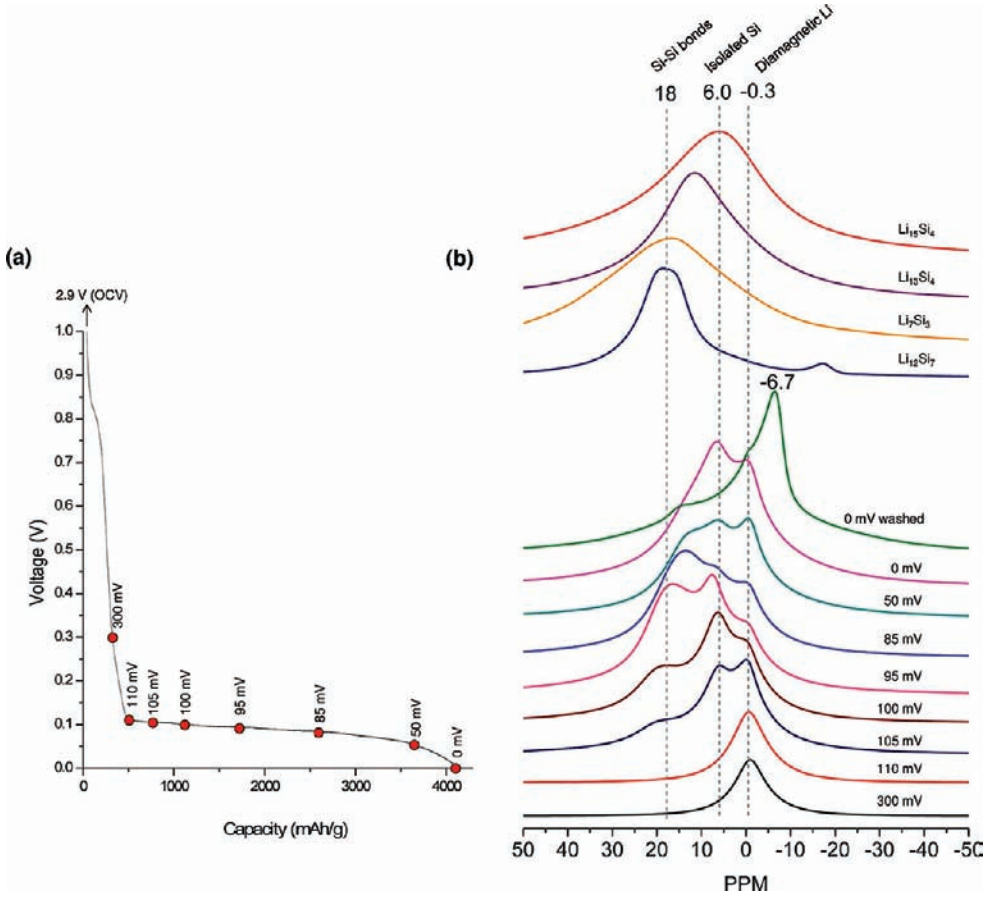


***Figure 5.*** (a) Electrochemical profile of the first discharge of crystalline silicon vs $Li/Li^+$ (the initial cell potential, (OCV, open circuit voltage) is marked with an arrow). (b) Ex situ $^7Li$ NMR spectra of battery samples stopped at different potentials during first discharge of crystalline Si vs $Li/Li^+$.

electrode were stopped at different potentials, and the electrode materials were extracted (Figure 5a). The batteries arrested at 300 and at 110 mV, give rise to a resonance at −0.3 ppm (Figure 5b), which is assigned to diamagnetic environments for Li in carbon ($Li_xC$), in the (dried) electrolyte solution, in the solid electrolyte interphase (SEI)[22] and possibly in environments created due to reaction with oxides on the surface of the silicon. The −0.3 ppm resonance is present in NMR spectra of all of the electrode samples extracted from actual batteries (Figure 5b).

After 110 mV, the reaction of crystalline silicon with lithium takes over, and new $^7Li$ resonances start to appear (Figure 5b). At 105 mV (250 mA h $g^{-1}$, after the capacity of the carbon process has been accounted for, i.e., 0.26 Li inserted per Si) two distinct peaks are observed at 18.0 and 6.0 ppm, which are assigned to lithium ions surrounding small Si clusters (i.e., structures containing Si−Si bonds as found in chains/rings/dumbbells) and lithium ions near isolated silicon ions, respectively, which are formed on breaking up the crystalline silicon diamond structure. Based on the sizes of the clusters in the model compounds and the similarity of their NMR shifts to those seen here, this suggests that clusters first formed on lithiation similarly contain 2−5 silicon atoms. Based on the relative areas of the two resonances, lithium ions nearby the isolated silicon ions dominate over Li nearby Si−Si clusters. On further lithiation, the 18 ppm peak grows significantly until a potential of 95 mV is reached (1200 mA h $g^{-1}$, 1.25 Li inserted per Si), whereas the 6.0 ppm peaks grows only slightly, suggesting that both isolated silicon and the clusters form right in the beginning of the formation of the amorphous phase, but that as the lithiation continues, the rupturing of the Si lattice proceeds via the formation of smaller clusters. After 95 mV, the 18 ppm peak starts to shift to lower frequencies and decreases in intensity. This is consistent with the reaction of the Si−Si clusters with further Li to form more isolated Si ions. The presence of both clusters and isolated silicon anions in the 50 mV sample is consistent with the estimated Li content of the amorphous phase ($Li_{3.4\pm0.2}Si$), which based on the structure of the model compound with the closest lithium content, $Li_{13}Si_4$, will contain both these species. As the lithiation proceeds below 50 mV, more Si−Si bonds are broken and the spectrum of the sample extracted from the 0.0 V battery (3600 mA h $g^{-1}$, 3.75 Li inserted per Si) is dominated by the resonance at 6.0 ppm due to the isolated Si ions, consistent with the formation of the crystalline $Li_{15}Si_4$ phase (Figure 5b).

**3.2.2. In Situ NMR.** In order to directly monitor the changes that occur in the LIB in real time, a flexible in situ crystalline silicon vs $Li/Li^+$ battery (Figure 2, a and b) was fully discharged and then charged, with a C/75 rate, in a conventional static NMR probe, during $^7Li$ NMR data acquisition (Figure 6). A recycle delay of 0.2 s was chosen since it partially suppresses the signal from the diamagnetic Li due to salts in the electrolyte, which has a spin lattice relaxation time, $T_1$ (as measured in an inversion recovery experiment) of approximately 300 ms. The four lower Li content lithium silicide model compounds have $T_1$'s of 100−157 ms (18 ppm resonance = 101−108 ms; 0−6 ppm, 144−157 ms). The $T_1$ of $Li_{21}Si_5$ is even shorter (50−60 ms). The initial spectrum at the beginning of the electrochemical cycle shows four small peaks at around at 0−8 ppm (Figure 6, A1). The smallest feature at lower frequency is due to the lithium ions in the electrolyte solution (black), and the two peaks (light

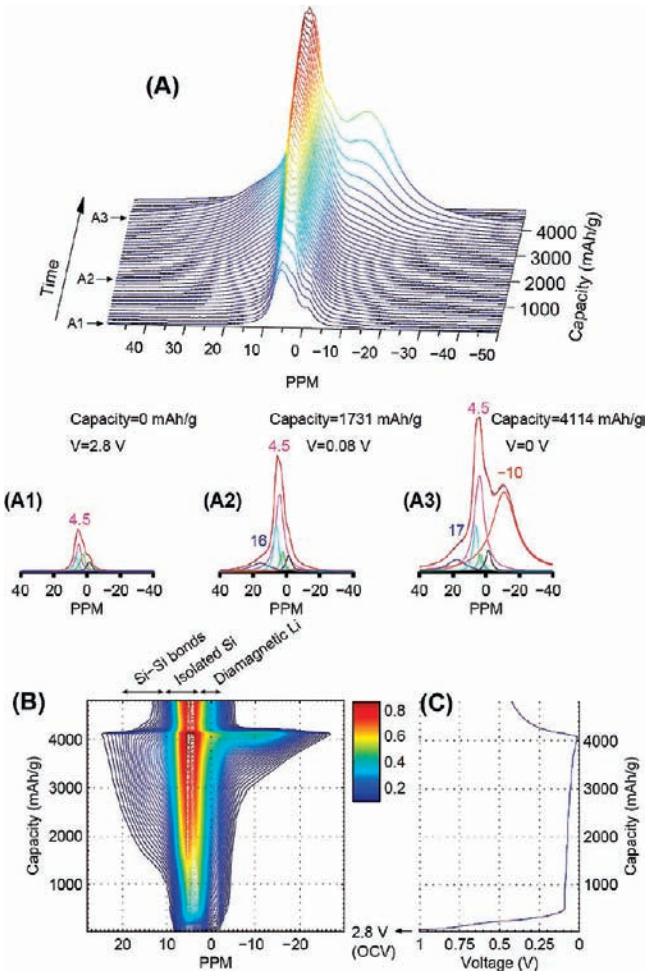


***Figure 6.*** Stacked (A) and contour (B) plots of in situ $^7$Li static NMR spectra and electrochemical profile of the first discharge (C) of an actual crystalline Si vs Li/Li$^+$ battery (the color bar shows the relative intensity scale for the spectra). A1−A3. Deconvoluted spectra at various discharge capacity values of interest.

blue and green) at higher frequencies are ascribed to lithium in passivation (SEI) layers on both the positive and negative electrodes[25] and in $Li_xC$ (see the Supporting Information for a fuller discussion concerning the peak fitting). Upon discharging, a broad peak appears at around 18 ppm at approximately 500 mA h g$^{-1}$ (i.e., immediately following the carbon process), which is ascribed to the formation of small silicon clusters. The peak grows and shifts to lower frequencies (Figure 6, A2) along the electrochemical plateau until 0.055 V, where it reaches 14 ppm (3000 mA h g$^{-1}$, see Supporting Information). A resonance is also observed at approximately 4.5 ppm, which grows steadily with time, particularly from 0 to 1250 mA h g$^{-1}$. This peak (magenta in A1−A3) is ascribed to formation of isolated silicon clusters, but it also contains an (overlapping) contribution from resonances from the SEI/$Li_xC$ Li environments. The much stronger intensity of the 4.5 ppm resonance over that from the 18−14 ppm resonance from 100 to 50 mV (see Figure 6, A1, A2 and A3) reflects the dominance of the formation of isolated Si atoms over the formation of Si−Si clusters. Even though the resolution is poorer in the static, as compared to the MAS NMR spectra, the data largely agree with the ex situ data, until close to the end of the discharge. The small shifts of some of the resonances between the two methods are ascribed to (a) the fact that the static peak maximum does not always correspond to the isotropic shift and (b) small susceptibility shifts of the $^7$Li signals due largely to the presence of metal components in the LIBs such as the Li metal and current collectors.

At the bottom of the discharge (below 30 mV), i.e., when the crystalline phase $Li_{15}Si_4$ is seen by XRD, a new peak appears at −10 ppm (Figure 6, A3); this is accompanied by the loss of intensity of the 17 ppm resonance, and a noticeable slowing down of the growth in intensity of the 4.5 ppm resonance. The negative shift suggests the formation of a highly shielded lithium environment (relative to the environment of the reference Li environment, $Li^+$ (aq), which resonates at 0 ppm). The intensity of the −10 ppm resonance is enhanced relative to the other resonances due to the short relaxation time of this signal (approximately 33 ms). The intensity of the −10 ppm peak decreases extremely rapidly upon charging the battery in the in situ NMR experiments, and upon removing only approximately 0.16 Li per formula unit (150 mA h g$^{-1}$) the voltage has increased to 300 mV, and the intensities of both the resonances at approximately 4.5 and 17 ppm increase (see Supporting Information).

One major issue that must now be resolved is the apparent inconsistency between the ex- and in situ results, at low voltages. This issue was resolved by investigating a second battery that had been fully discharged ex situ. Upon stopping the discharge current at the bottom of the discharge (0.0 V), and monitoring the evolution of the resonances in situ, the environment giving rise to the −10 ppm resonance was seen to slowly disappear as the battery relaxes over a period of approximately 10 h (Figure 7A). This is ascribed to a reaction between the clearly very reactive, metastable, "$Li_{15}Si_4$" phase with the electrolyte, via a "self-charge" mechanism. [N.b., in a battery where silicon is the negative electrode (e.g., $LiCoO_2$ vs Si) this will manifest itself as a self-discharge mechanism.] This signal returns on a subsequent discharge of the *same* battery.

Once this self-discharge process was identified, we were then able to extract the short-lived, reactive phase from the coin cell battery by shorting the positive and the negative electrodes of the battery while transferring the battery into the inert atmosphere of a glovebox. The lithiated phase was then quickly extracted, washed and packed into rotors for ex situ $^7$Li MAS NMR analysis. Now the spectrum is dominated by a resonance at negative frequencies (−6.7 ppm), consistent with the in situ NMR data (Figure 5b, 0 V washed).

The $^7$Li signal of $Li_{15}Si_4$ synthesized directly from the elements by ball-milling and the new phase formed electrochemically, clearly have different electronic structures, based on their very different NMR shifts. However, no obvious differences were seen in the diffraction patterns of the two compounds, suggesting that the long-range ordering of at least the silicon ions is similar. Even after the self-discharge process, the "$Li_{15}Si_4$" crystalline phase is still observed in the XRD pattern (see Supporting Information); however, the −10 ppm is no longer seen, and the spectrum is similar to that observed in the ex situ NMR experiment for the (unintentionally) relaxed cell (Figure 5, 0 V). Some insight into these phenomena can be obtained by considering the isostructural material $Li_{15}Ge_4$. This is a somewhat unusual electron-deficient phase, since it lacks one electron per formula unit ($Li^+{}_{15}Ge^{3.75-}{}_4$). The stability of $Li_{15}Ge_4$ was rationalized based only on the relative instability

(25) Meyer, B. M.; Leifer, N.; Sakamoto, S.; Greenbaum, S. G.; Grey, C. P. *Electrochem. Solid State Lett.* **2005**, *8*, A145−A148.
(26) Zhukovskii, Y. F.; Balaya, P.; Kotomin, E. A.; Maier, J. *Phys. Rev. Lett.* **2006**, *96*, 058302.

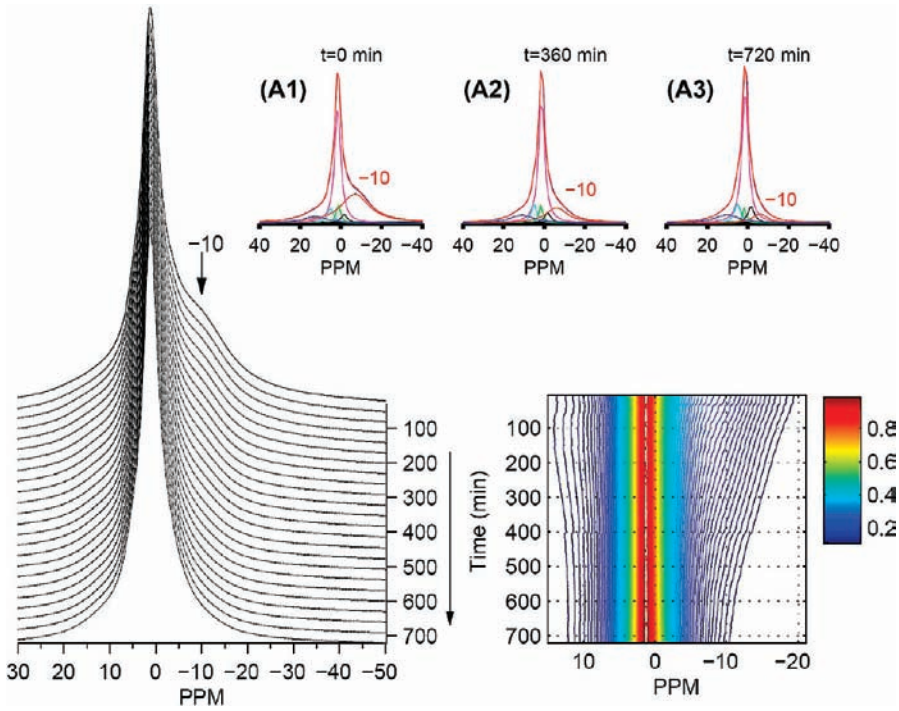


***Figure 7.*** Stacked (A) and contour (B) plots of in situ $^{7}$Li static NMR spectra of the relaxation of a crystalline Si vs Li/Li$^{+}$ battery stopped at the end of the full discharge (0 V) (the color bar shows the relative intensity scale for the spectra in the contour plot). (Al−A3) Deconvoluted spectra at different relaxation times.

of the nearby $Li_{21}Ge_5$ phase.[7] In contrast, isostructural $Li_{14}MgSi_4$ is a normal Zintl phase with the following formal charges $Li^{+}_{14}Mg^{2+}Si^{4-}_{4}$. Taken together, this suggests that this structure type can accommodate excess charge. Our experimental data indicate that "$Li_{15}Si_4$" is not a line phase but rather can accommodate some nonstoichiometry, which is in agreement with previous work.[2] The phase observed for the ball milled model compound and the one that first forms in a LIB has a stoichiometry corresponding to $Li_{15}Si_4$, or possibly $Li_{15-\delta'}Si_4$, if the initial phase is slightly Li deficient, while the phase associated with the resonance at −10 ppm corresponding to $Li_{15+\delta}Si_4$, the range of nonstoichiometry being given by $\delta + \delta'$. This suggestion is explored below.

## 4. Investigation of $Li_{15}Si_4$ Nonstoichiometry and $Li_{15}Si_4$-Electrolyte Reactions

A number of methods were used to attempt to quantify the range of nonstoichiometry and reactivity of the metastable phase, "$Li_{15}Si_4$" formed electrochemically and by ball-milling. First, on the basis of the capacity required to remove the −10 ppm peak seen in the in situ NMR experiments on charging the cell (Figure 6, B and C), the nonstoichiometry corresponds to approximately 0.16 Li per formula unit (per Si). A previous diffraction study has shown that the $Li_{15}Si_4$ crystalline phase is still present at this composition.[16] In a second method, a coin cell battery was discharged fully and then rested for 320 h. The open circuit potential (OCV) is plotted vs time in Figure 8. The initial rise in the OCV up to 0.12 V over 10 h is attributed to the reaction of the metastable phase, "$Li_{15}Si_4$" with the electrolyte. After the rest step, the cell was discharged fully a second time, requiring an additional 140 mA h g$^{-1}$, corresponding to 0.145 Li per Si, i.e., $(\delta + \delta') = 0.55-0.60$. This excess discharge capacity is presumably required to compensate for the loss of Li from the metastable phase during the rest step. N.b., the unstable OCV even after the 320 h rest step suggests that the reaction may still be incomplete, consistent with the slightly

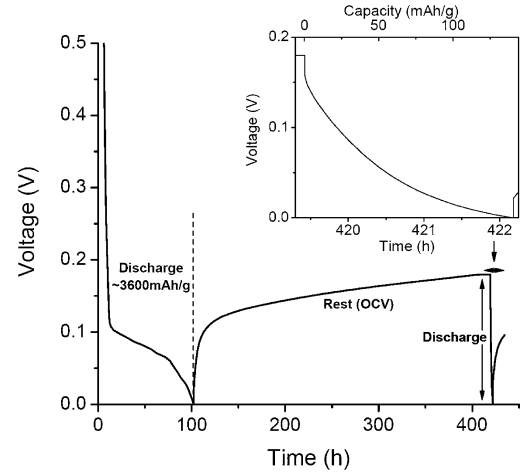


***Figure 8.*** Electrochemical plot of crystalline silicon vs Li$^{+}$/Li. The open circuit potential is plotted during the rest period (after the first discharge). (Inset) Magnified plot of the second discharge after the rest step.

lower lithium nonstoichiometry that is obtained from this method, in comparison to that estimated based on the capacity associated with the loss of the −10 ppm resonance, as seen by in situ NMR spectroscopy.

The model compound $Li_{15}Si_4$, synthesized by ball-milling, was made into an electrode and electrochemically discharged to a potential of 0 V and washed. The $^{7}$Li NMR shift of this discharged sample is clearly more shielded than that of pristine $Li_{15}Si_4$, as shown in Figure 9, consistent with additional lithium insertion in this phase. This provides additional evidence that $Li_{15}Si_4$ is not a line phase and can accommodate a slight excess of lithium. However, the resonance does not shift to as low a frequency as observed following electrochemical lithation of Si (Figure 5b, −6.7 ppm). This may be due to the variations in the ability of the two $Li_{15}Si_4$ materials, one synthesized by ball-

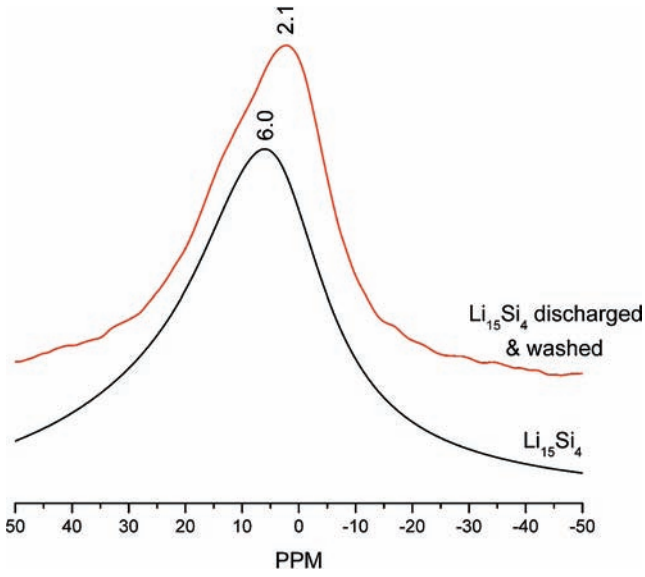


***Figure 9.*** $^{7}$Li MAS NMR spectra collected at 38 kHz spinning speed of pristine $Li_{15}Si_4$ and a $Li_{15}Si_4$ sample fully discharged and then washed.

milling and the other electrochemically, to accommodate additional Li, due to differences in particle sizes and/or defect concentrations. Alternatively, some partial self-discharge of the overlithiated $Li_{15}Si_4$ (ball-milled) phase could have occurred before the cell was taken apart. Consistent with this, a shoulder at 15 ppm in the spectrum of the discharged material is seen, suggesting the formation of Si−Si small clusters formed via a self-discharge process. This further suggests that $Li_{15}Si_4$ can react with the electrolyte to form an amorphous lithium silicide phase.

Finally, we investigated the effect of binder on the low-voltage process. Figure 10 shows the comparison between the OCV of cells constructed with and without the use of CMC binder[1] that have been left to relax following the first full discharge process. The electrochemical profile of the CMC cell shows that the cell still relaxes but the initial rise in the OCV is smaller. The CMC cell reaches only 75 mV after 9 days, whereas the OCV of the cell with no binder rises much more rapidly, reaching 170 mV. In contrast a CMC cell took almost a month (29 days) until it reached 170 mV. Although the initial rise in OCV for the CMC cells varies slightly between cells, the two electrochemical profiles shown in Figure 10 represents the lower and upper limits of the OCVs observed in several CMC cells. The initial rise in the potential profile always remained below 100 mV for CMC cells and above 100 mV for cells with no binder. Figure 10b shows that the ex situ NMR spectra acquired for the fully discharged CMC cell contains the approximately −5 ppm resonance, but that the 9 day relaxed

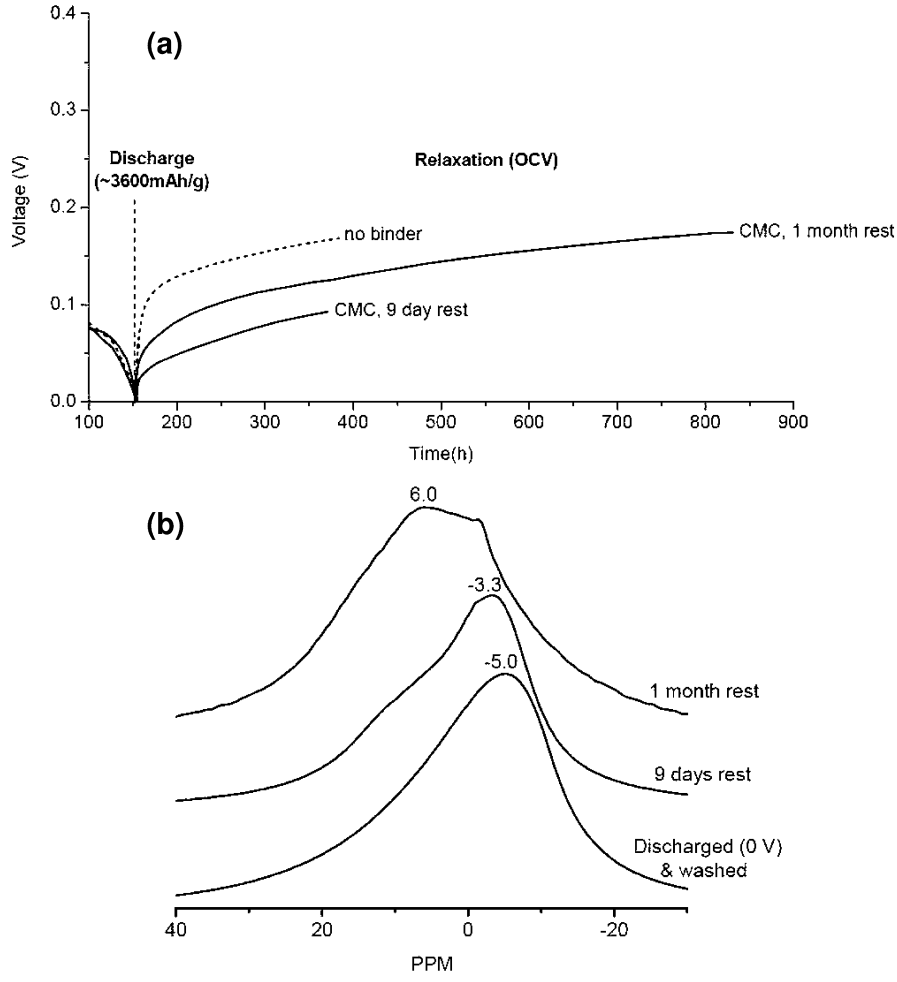


***Figure 10.*** (a) Electrochemical profiles of the first discharge, followed by either 9 days or 1 month relaxation of crystalline silicon vs $Li/Li^+$ cells prepared with (solid lines) and without CMC binder (dashed line, 9 days relaxation). The first 100 h of the discharge are not shown. (b) Ex situ $^{7}$Li NMR spectra of battery samples stopped at the end of the first discharge (0 V), after 9 days and 1 month relaxation of crystalline Si vs $Li/Li^+$, prepared with a CMC binder.

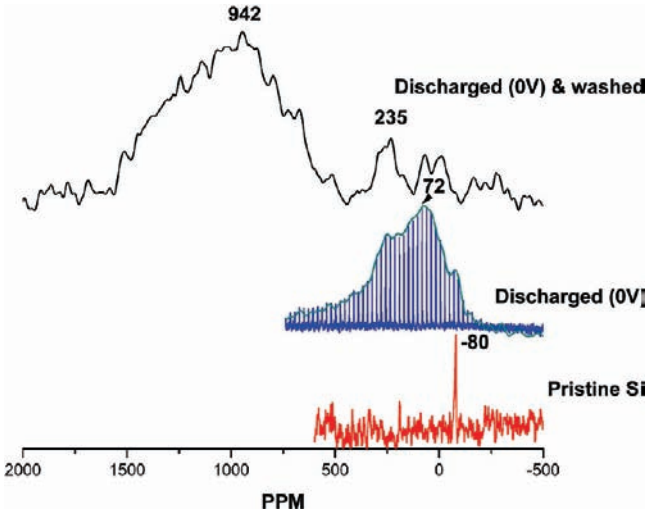


***Figure 11.*** $^{29}$Si MAS NMR spectra of crystalline silicon, fully discharged crystalline silicon and a fully discharged and immediately washed sample. Spectra were collected at a 14 kHz spinning speed, and a CPMG sequence was used for the fully discharged sample (unwashed).

CMC cell still has a resonance at −3.3 ppm suggesting the relaxation is not complete. The relaxation of the CMC cell that was allowed to rest for a month is close to completion, and the negative ppm resonances are replaced by a resonance at 6 ppm. In contrast to binders such as PVDF, CMC had been suggested to bond to the thin layer of $SiO_2$ on the Si particles, which results in better accommodation of the expansion/shrinkage upon cycling Si.[1] Such a coating also appears to inhibit the reaction of the highly reactive $Li_{15+\delta}Si_4$ with the electrolyte.

Analysis of the in situ NMR experiments suggests that the side reactions also occur between the lithium silicides and the electrolyte at higher voltages. The effect of these reactions is, however, much easier to monitor at very low voltages, because it results in significant changes in both the NMR spectrum and the OCV. However, the intensity of the 4.5 ppm $^7$Li resonance, which we have assigned to both Li in the SEI and nearby isolated Si atoms, continues to grow steadily with time, even during the initial stages of the discharge and on charge (where Li should be removed from the lithiated silicide, reducing the intensity of this resonance). This confirms that some of this signal is due to products arising from electrolyte decomposition, and indicates that the amorphous lithium silicides are also reactive. Additional in situ experiments (not shown) showed that the 4.5 ppm peak did not gain in intensity when the battery was discharged to only 100 mV and left for a day. More detailed NMR experiments are in progress to attempt to separate some of the overlapping signals from the different components in the static spectra of the intact batteries and to investigate the decomposition reactions in greater detail. Finally, our batteries used for the in situ NMR studies were only associated with capacities for the first charge of approximately 1500 mA h $g^{-1}$, the capacity dying rapidly on subsequent cycles. This capacity fade may be inherent to the binder choice used in the in situ NMR cell, and the likely related reactions with the electrolyte. We are attempting to optimize our design to allow studies of multiple discharge−charge cycles.

## 5. Silicon-29 MAS NMR of the Discharged Samples

In order to probe the changes in electronic structure, as monitored at the Si sites, ex situ $^{29}$Si NMR experiments are presented (Figure 11) from two of the samples whose $^7$Li spectra were shown in Figure 5b. They clearly show a change in the silicon local structure on lithiation, as most of the intensity at −80 ppm from crystalline silicon is converted to broad resonances at 72 and 235 ppm, for the cell disassembled at the end of the discharge step, without washing. However, if the electrode (of the discharged cell) is quickly washed and packed into the rotors for data acquisition, a significant shift of the Si resonance is seen and a new, broad peak centered at 942 ppm is observed. Very little signal is present between 72 and 235 ppm. This again confirms that the electronic structure surrounding the Si in the $Li_{15+\delta}Si_4$ is very sensitive to whether the sample is allowed to rest before disassembling the cell, consistent with the $^7$Li NMR results. Finally, space-charge mechanisms have been used to explain additional capacity in some nanocomposites.[26] These results do not appear to be consistent with this mechanism, since essentially all of the $^{29}$Si signal is shifted, and not just the signals from Si atoms near the surface of the particles.

## 6. Conclusions

A combination of in- and ex situ NMR has been used to investigate the structure of the amorphous phase. The process in the first discharge occurs via the lithiation of Si to form isolated Si and Si−Si clusters. The Si−Si clusters are then broken apart at the end of the first discharge to form isolated Si ions and eventually the crystalline phase. The crystalline phase does not appear to be a line phase, at least in the composite battery electrode. Instead it can accommodate a small excess of Li. This excess-Li phase is extremely reactive in the electrolyte and the Li−Si cell "self-discharges", leading to the loss of Li from this phase, and an accompanying increase in the open circuit voltage. The amorphous lithium silicides also appear to be reactive and the self-discharge mechanisms at lower stages of discharge are currently under investigation, along with a more detailed analysis of the changes that occur during the first charge and in subsequent discharge−charge cycles.

The self-discharge mechanism could represent a mechanism for capacity loss in Si batteries if they are discharged to too low voltages, which can occur if the batteries are cycled at too high rates. Furthermore, the reactivity of this phase may also be a safety concern. However, our preliminary experiments indicate that CMC inhibits this discharge process significantly, cells taking days to months to relax. These results indicate that the strong binding of CMC to silicon is important in preventing capacity loss due to side reactions with the electrolyte. Finally, the results highlight the ability of in situ NMR methods to capture dynamic processes that are not straightforward to observe by using ex situ NMR methods. A wide range of different applications of the method to investigate different LIB electrode materials and intercalation/conversion processes, along with side-reactions such as those associated with SEI formation can be foreseen.

**Acknowledgment.** This work was supported by the Assistant Secretary for Energy Efficiency and Renewable Energy, Office of Freedom CAR and Vehicle Technologies of the U.S. DOE under Contract No. DE-AC03-76SF00098, via subcontract No. 6517749 with the Lawrence Berkeley National Laboratory and funding from the New York State Foundation for Science, Technology and Innovation NYSTAR award, and the NSF via DMR0804737. This work has benefited from the use of the Advanced Photon Source at Argonne National Laboratory. We thank Jean-Sebastien Bridel, Peter Chupas, Evan Maxey and Fulya Dogan for experimental support.

**Supporting Information Available:** In situ X-ray diffraction of the first discharge of crystalline silicon vs $Li/Li^+$ and ex situ X-ray diffraction of selected battery samples at different states of discharge and following relaxation, discussion of shifts and peak assignments for the $^7Li$ NMR of the thermodynamic phases, plots of intensities and peak shifts of deconvoluted peaks observed in in situ NMR experiments and a movie of the in situ NMR data synchronized with the electrochemical plot. This material is available free of charge via the Internet at http://pubs.acs.org.

JA8086278